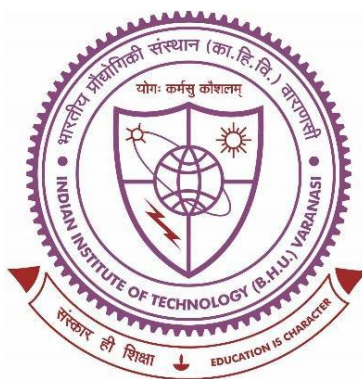


Exploring Therapeutic Approaches for Targeted Delivery of Cabazitaxel in Breast Cancer Therapy



Thesis submitted in partial fulfilment for the
Award of Degree

Doctor of Philosophy

By

Abhishek Jha, M. Pharm

**Department of Pharmaceutical Engineering & Technology
Indian Institute of Technology
(Banaras Hindu University)
Varanasi-221005, India**

Roll No. 19161002

Year: 2024



CERTIFICATE

It is certified that the work contained in the thesis titled “**Exploring Therapeutic Approaches for Targeted Delivery of Cabazitaxel in Breast Cancer Therapy**” by **Mr. Abhishek Jha** has been carried out under my supervision and that this work has not been submitted elsewhere for a degree.

It is further certified that the student has fulfilled all the requirements of Comprehensive Examination, Candidacy and SOTA for the award of Ph.D. Degree.

**Prof. Brahmeshwar Mishra
(Supervisor)**

Dr. B. Mishra

Professor of Pharmaceutics
Department of Pharmaceutical
Engineering And Technology
Indian Institute of Technology
(Banaras Hindu University)
Varanasi-221005

Date: 27.03.2025

Place: IIT (BHU), Varanasi



DECLARATION BY THE CANDIDATE

I, **Abhishek Jha**, certify that the work embodied in this Ph.D. thesis is my own bonafide work and carried out by me under the supervision of **Prof. Brahmeshwar Mishra** from **July, 2019 to December, 2024** at the **Department of Pharmaceutical Engineering & Technology, Indian Institute of Technology (Banaras Hindu University), Varanasi**. The matter embodied in this Ph.D. thesis has not been submitted for the award of any other degree/diploma. I declare that I have faithfully acknowledged and given credit to the research workers wherever their works have been cited in my work in this thesis. I further declare that, I have not willfully copied any other's work, paragraphs, text, data, results, etc. reported in the journals, books, magazines, reports, dissertations, theses, etc., or available on websites and have not included them in this Ph.D. thesis and have not cited as my own work.

Date: 27.3.25
Place: IIT (BHU), Varanasi


Abhishek Jha

CERTIFICATE BY THE SUPERVISOR(S) AND HEAD OF THE DEPARTMENT

It is certified that the above statement made by the student is correct to the best of our knowledge.


Prof. Brahmeshwar Mishra
(Supervisor)
Dr. B. Mishra
Professor of Pharmaceutics
Department of Pharmaceutical
Engineering And Technology
Indian Institute of Technology
(Banaras Hindu University)
Varanasi-221005


Prof. Sairam Krishnamurthy
(Head of the Department)
विभागाध्यक्ष / Head
भैषजकीय अभियांत्रिकी एवं प्रौद्योगिकी विभाग /
Department of Pharmaceutical Engineering & Technology
भारतीय प्रौद्योगिकी संस्थान / INDIAN INSTITUTE OF TECHNOLOGY
(बनारस हिन्दू विश्वविद्यालय) / (BANARAS HINDU UNIVERSITY)
वाराणसी-२२१००५ / Varanasi-221005

Department of Pharmaceutical Engineering & Technology

Indian Institute of Technology
(Banaras Hindu University)
Varanasi-221005



COPYRIGHT TRANSFER CERTIFICATE

Title of the Thesis: Exploring Therapeutic Approaches for Targeted Delivery of Cabazitaxel in Breast Cancer Therapy

Candidate's Name: Mr. Abhishek Jha

Copyright Transfer

The undersigned hereby assigns to the Indian Institute of Technology (Banaras Hindu University), Varanasi all rights under copyright that may exist in and for the above thesis submitted for the award of the Ph.D. degree.

Date: 27.3.25

Place: IIT (BHU), Varanasi

Abhishek Jha

Note: However, the author may reproduce or authorize others to reproduce material extracted verbatim from the thesis or derivative of the thesis for author's personal use provided that the source and University's copyright notice are indicated.

Acknowledgement

I am deeply grateful to Bharat Ratna Pandit Madan Mohan Malviya ji for his unwavering dedication in establishing the esteemed institution, Banaras Hindu University. His tireless efforts have created this sacred space of learning, and I feel privileged to be a part of it.

I extend my sincere gratitude to my supervisor, Prof. Brahmeshwar Mishra, for his unwavering support and guidance throughout my Ph.D. research journey. His extensive knowledge, vast research experience, and invaluable suggestions have been instrumental in shaping the trajectory of my work. His insightful feedback challenged me to refine my thinking and elevate the quality of my research. I am truly thankful for the opportunity to be his student, and for the enduring faith he has shown in me over the years. I find it challenging to express adequately my appreciation for his role in shaping me into not only a better researcher but also a better person.

I extend my sincere thanks to Prof. Sairam Krishnamurthy, Head of the Department of Pharmaceutical Engineering & Technology, I.I.T. (B.H.U.), Varanasi, for his invaluable support in providing the necessary infrastructure facilities throughout the course of my work.

I would like to extend my sincere thanks to RPEC member Dr. Ruchi Chawla from the Department of Pharmaceutical Engineering & Technology), and Dr. Abha Mishra from the School of Biochemical Engineering. Their valuable input and constructive criticism have played a pivotal role in encouraging me to broaden the scope of my research from various perspectives.

I would like to thank Prof. M. S. Muthu, Dr. Ashish Agarwal, Dr. Shreyans K Jain, and Dr. Dinesh Kumar for providing access to their lab facilities. Also, Dr. Vinod Tiwari for providing the necessary resources and guidance to carry out in vivo experiments.

I extend my heartfelt thanks to all the esteemed faculty members of the department, including Prof. Sushil K Singh, Prof. Sushant K. Srivastava, Prof. S. Hemalatha (Former Head), Prof. A. Senthil Raja, Dr. Ashok Kumar, Dr. Alakh. N Sahu, Dr. Sunil. K. Mishra, Dr. Prasanta Kumar Nayak, Dr. Gyan Prakash Modi, Dr. Deepak Kumar, and Dr. Jairam Mishra. Their unwavering support and encouragement have been instrumental during the progress of my research, and I am sincerely grateful for their kindness and guidance.

The support and the resources provided by Central Instrument Facility (CIF), IIT(BHU), Varanasi and Sophisticated Analytical & Technical Help Institute, Banaras Hindu University (SATHI-BHU) are gratefully acknowledged.

I pay sincere thanks to Mr Yashwant Singh, Mr Atul Gupta, Mr Anand and all the departmental non-teaching staff for their co-operation and help during my research work. I am thankful to the Ministry of Education, GoI, for providing support in the form of a teaching assistantship.

I want to express my heartfelt thanks to my amazing friends. Your constant encouragement and support have played a crucial role in making this work a reality. Having friends like you by my side has made the journey not only memorable but also achievable.

I would like to extend my deepest gratitude to my family. Without their unwavering support, encouragement, and love, achieving this would not have been possible. Their belief in me has been my source of strength and motivation throughout this journey. Thank you for being my pillars of support and for making this achievement a reality.

Date: 27.3.25

Place: IIT(BHU) Varanasi

Abhishek
Abhishek Jha

Table of Contents

1	Introduction	2
1.1	Biopolymers for the design of tumor microenvironment responsive systems	3
2	Literature Review	6
2.1	Biopolymers with pH-responsive cleavage bonds	7
2.2	Biopolymers with pH-responsive protonated chemical groups	10
2.3	Biopolymers with Cleavable ROS responsive bond	10
2.4	Biopolymers with amphiphilicity transition-ROS responsive bond.....	13
2.5	Biopolymers with enzyme responsive bonds	16
2.6	Biopolymers with hypoxia activatable groups	18
2.7	Cleavable-bond based targeting	23
2.8	pH-dependent Protonation mediated targeting	26
2.9	Size dynamic targeting	27
2.10	Charge reversal targeting	27
2.11	Redox responsive nanomedicine	30
2.12	Enzyme responsive nanomedicine.....	33
2.13	Hypoxia responsive nanomedicine	35
2.14	Dual stimuli-responsive nanomedicine.....	37
2.15	Stimuli activated surface ligand-mediated targeting.....	38
2.16	Limitations	45
2.17	Carriers for localized delivery of TME-Responsive nanomedicine	46
3	Objectives and Plan of Work.....	50
3.1	Objectives	50

3.2	Plan of Work.....	50
3.2.1	Cetuximab functionalized chitosan/hyaluronic acid-based nanoparticles loaded with cabazitaxel for enhancing anti-tumor efficacy in DMBA-induced breast cancer model in rats through spatial targeting	50
3.2.2	Cabazitaxel-loaded redox-responsive nanocarrier based on D-alpha-tocopheryl-chitosan and hyaluronic acid loading for improved anti-tumor efficacy in DMBA-induced breast cancer model.....	51
3.2.3	Hyaluronic acid-oleylamine and chitosan-oleic acid conjugate-based hybrid nanoparticle delivery via. dissolving microneedles for enhanced treatment efficacy in localized breast cancer	52
4	Cetuximab functionalized chitosan/hyaluronic acid-based nanoparticles loaded with cabazitaxel to improve the anti-tumor efficacy in DMBA-induced breast cancer models in rats	54
4.1	Introduction	54
4.2	Materials and Methods	56
4.2.1	Materials	56
4.2.2	Synthesis and characterization of succinylated TPGS.....	57
4.2.3	Preparation of chitosan/hyaluronic acid-based nanoparticles.....	58
4.2.4	Physicochemical characterization of nanoparticles	60
4.2.5	Analytical method development	61
4.2.6	Encapsulation efficiency, drug loading, and degree of conjugation	61
4.2.7	Drug release study.....	62
4.2.8	In vitro cell line studies.....	63
4.2.9	In vivo studies in female Sprague Dawley rats.....	66
4.2.10	Statistics	67

4.3	Results and Discussion	67
4.3.1	Characterization of succinylated TPGS	67
4.3.2	Characterization of nanoparticles.....	79
4.3.3	Drug release study	86
4.3.4	In vitro assessment of nanoparticle efficacy	88
4.3.5	In vivo studies	96
5	Cabazitaxel-loaded redox-responsive nanocarrier based on D-alpha-tocopheryl-chitosan and hyaluronic acid for improved anti-tumor efficacy in DMBA-induced breast cancer model	106
5.1	Introduction	106
5.2	Materials and Methods	109
5.2.1	Materials.....	109
5.2.2	Synthesis and Characterization of TPGS-COOH and CSVE	110
5.2.3	Formulation of CSVE-based nanoparticles.....	111
5.2.4	Characterization of CSVE-based nanoparticles	112
5.2.5	Drug release Study	114
5.2.6	Stability of lyophilized nanoparticles.....	115
5.2.7	In vitro cell line studies	115
5.2.8	In vivo Studies	118
5.2.9	Statistical Analysis	121
5.3	Results and Discussion	121
5.3.1	Synthesis of TPGS-COOH and CS-VE	121
5.3.2	Formulation and characterization of CSVE-based nanoparticles	125
5.3.3	Drug release Study	133

5.3.4	In vitro Study	139
5.3.5	In vivo Studies	151
6	Hyaluronic acid-oleylamine and chitosan-oleic acid conjugate-based hybrid nanoparticle delivery via dissolving microneedles for enhanced treatment efficacy in localized breast cancer	162
6.1	Introduction	162
6.2	Materials and methods	164
6.2.1	Materials required	164
6.2.2	Synthesis of CS-OA, HA-OA, and TPGS-COOH.....	165
6.2.3	Characterization of CS-OA, HA-OA, and TPGS-COOH.....	167
6.2.4	Synthesis of HA-OA/CS-OA based nanoparticles.....	167
6.2.5	Fabrication of Microneedle.....	169
6.2.6	Characterization of HA-OA/CS-OA based nanoparticles.....	171
6.2.7	In vitro drug release of HA-OA/CS-OA based nanoparticles.....	173
6.2.8	Cell culture studies.....	173
6.2.9	Evaluation of MN	175
6.2.10	In vivo efficacy: tumor regression, survival analysis, and histological studies 177	
6.2.11	Statistical analysis.....	177
6.3	Results and discussion.....	178
6.3.1	Synthesis and characterization of CS-OA, HA-OA, and TPGS-COOH	178
6.3.2	Formulation and characterization of nanoparticles.....	182
6.3.3	In vitro drug release study.....	189
6.3.4	Cell culture studies.....	190

6.3.5	Fabrication and evaluation of dissolving MN.....	196
6.3.6	In vivo studies	201
7	Summary and conclusions	208
7.1	Future perspective	210
	References.....	212
8.	Appendices.....	256

List of Figures

Figure 1.1 Graphical illustration of the precise therapeutic delivery mechanism of biopolymer-based nanomedicine tailored to exploit tumor microenvironment stimuli. ____	4
Figure 2.1 Mechanism of pH-responsive behavior of Dimethylacrylamide-Trimethyl chitosan; At acidic pH, DMMA-TCM exhibits imine bond cleavage resulting in dissociation of dimethylacrylamide and Trimethyl-chitosan [2]. _____	7
Figure 2.2 Synthetic route of N-succinyl-CS and Al-CS [4]. _____	8
Figure 2.3 Synthesis of dual pH and redox-sensitive acrylic polymer conjugated thiolated chitosan [5]. _____	9
Figure 2.4 Synthesis of pH and redox-sensitive DOX/ α -TOS-HMSN-TK-CMCH-GRP78P [15]. _____	12
Figure 2.5 Synthesis of ROS sensitive amphiphilic Poly(propylene sulfide) grafted Chondroitin sulfate (ChS) polymer ChS-g-PPS [16]. _____	14
Figure 2.6 Synthesis of ROS-sensitive thioether-bearing polymer and mechanism of ROS mediated increased hydrophilicity [10]. _____	15
Figure 2.7 Synthesis of redox-sensitive and CD44 receptor-targeted HASF polymer [21]. _____	16
Figure 2.8 Synthesis of hypoxia-sensitive nitroimidazole modified chitosan (Cs-NA) [31]. _____	19
Figure 2.9 Synthesis of a 2-nitroimidazole modified carboxymethyl dextran by EDC/NHS mediated carbodiimide chemistry [33]. _____	20
Figure 2.10 Synthesis of pH-sensitive adamantane-PEG _____	24
Figure 4.1 (A) Conjugation of SA with TPGS. (B) Schematic illustration of preparation of CS-HA-NP and CS-HA-Cmab-NP. _____	58

Figure 4.2 HPLC Chromatogram of Cabazitaxel (RT- 5.98 min) and Docetaxel (RT- 11.23)	61
Figure 4.3 Succinylation of TPGS	68
Figure 4.4 (A) FTIR, (B) DSC, and (C) XRD spectra of TPGS and TPGS-COOH	68
Figure 4.5 ¹ H NMR spectrum of TPGS Deuterated Methanol.	69
Figure 4.6 ¹ H NMR spectrum of TPGS-COOH Deuterated Methanol.	69
Figure 4.7 ¹³ C NMR spectrum of TPGS Deuterated Methanol.	72
Figure 4.8 ¹³ C NMR spectrum of TPGS-COOH in Deuterated Methanol.	72
Figure 4.9 Mass spectra of TPGS at {m/z (Da) = 300-1200}	74
Figure 4.10 Mass spectra of TPGS at {m/z (Da) = 600-1800}	75
Figure 4.11 Mass spectra of TPGS-COOH at m/z (Da) in the range of 300-1200	76
Figure 4.12 Mass spectra of TPGS-COOH at m/z (Da) in the range of 600-1800	77
Figure 4.13 Morphological assessment of CS-HA-NP and CS-HA-Cmab-NP by TEM, SEM and AFM.	80
Figure 4.14 (A) FTIR and (B) DSC spectra of neat CBT, CS, HA, TPGS-COOH, CS-HA-NP, and CS-HA-Cmab-NP.	82
Figure 4.15 XRD spectra of neat CBT, CS, HA, TPGS-COOH, CS-HA-NP, and CS-HA-Cmab-NP.	83
Figure 4.16 XPS spectra of CS-HA-NP and CS-HA-Cmab-NP.	85
Figure 4.17 The drug release profile of CS-HA-NP and CS-HA-Cmab-NP in Phosphate Buffered Saline pH 7.4, Phosphate Buffer pH 6.8, and Acetate Buffer pH 5.5. Comparative graph of release profiles of CS-HA-NP and CS-HA-Cmab-NP at various pH. Data presented as Mean ± SD (vertical bars); n=6.	86

Figure 4.18 Normalized cell viability of bCS-HA-NP, Neat CBT, CS-HA-NP, and CS-HA-Cmab-NP at various concentrations calculated by MTT assay. Data presented as Mean \pm SD (vertical bars); n=6. _____	89
Figure 4.19 Microscopic images of cells imaged using fluorescence microscope after treatment with Free C6, c6CS-HA-NP, and c6CS-HA-Cmab-NP for 6 h. Cells were counter stained with DAPI. Scale bar = 100 μ m. _____	90
Figure 4.20 Hoechst33342/PI-stained MDA-MB-231 cells after 24 h treatment with Neat CBT, bCS-HA-NP, CS-HA-NP, CS-HA-Cmab-NP. The yellow and red arrows represent early apoptotic and late apoptotic cells respectively. Cells emitting blue fluorescence are Hoechst positive while those with red fluorescence are PI positive. Scale bar= 100 μ m. _____	91
Figure 4.21 Microscopic images of JC-1-stained MDA-MB-231 cells after treatment with bCS-HA-NP, neat CBT, CS-HA-NP, and CS-HA-Cmab-NP. The control and bCS-HA-NP treated cells showed no signs of depolarization with cationic JC-1 binding to negatively charged polarized mitochondria to spontaneously form J-aggregates (red fluorescence). The CBT and CBT loaded nanoparticles show presence of JC-1 monomer (green fluorescence) due to depleted mitochondrial membrane potential Scale bar = 100 μm. _____	92
Figure 4.22 Images of MDA-MB-231 cells incubated with DCFH-DA after receiving various treatments for 24 h. The green fluorescence is due to the reduction of DCFH-DA to DCF in the presence of ROS (Scale bar = 400 μ m). _____	94
Figure 4.23 Cell cycle analysis; graphs showing population distribution of cells in different phases after incubation with various treatment for 24 h. _____	95
Figure 4.24 Comparative Plasma concentration vs time curve of Neat CBT, CS-HA-NP, and CS-HA-Cmab-NP. Data presented as Mean \pm SD (vertical bars); n=12. _____	97
Figure 4.25 Change in tumor volume in various treatment groups during 21-day treatment period. Data presented as Mean \pm SD (vertical bars); n=5 _____	98

Figure 4.26 Images of tumors collected from animals after 21-day treatment. In-image cm-scale on left side. _____	99
Figure 4.27 Average body weight of various treatment groups during the 21-day treatment period. Data presented as Mean \pm SD; n=5. *** (p-value < 0.001), **** (p-value < 0.0001), ns (p-value > 0.05)_____	99
Figure 4.28 Kaplan Meier survival plot of various treatment groups (up to 120 days). _	101
Figure 4.29 H&E-stained histological images of normal and tumor tissue after 21-day treatment period (images shown are captured with 4X lens). _____	101
Figure 4.30 H&E-stained histological images of organs collected from various treatment groups after 21-day treatment period (images shown are captured with 4X lens). _____	102
Figure 4.31 Graphical Summary of Objective 1 _____	104
Figure 5.1 Schematic representation of Synthesis of CSVE (A) and TPGS-COOH (B); Preparation of CSVE/HA-based redox responsive nanoparticles (C). _____	110
Figure 5.2 FTIR spectra of TPGS, TPGS-COOH, CSO, and CSVE. _____	122
Figure 5.3 The ¹ H NMR spectra of CSO (black) and CSVE (blue)._____	123
Figure 5.4 The ¹³ C NMR spectra of CSO (black) and CSVE (blue). _____	124
Figure 5.5 Morphological assessment (TEM, SEM, and AFM) of CSO/HA NP, CSVE/HA NP, CSVE/HA/DTPA NP, and CSVE/HA/DTPA/Cmab NP. _____	128
Figure 5.6 The FTIR spectra of CBT, CSVE, TPGS, HA, CSVE/HA NP, CSVE/HA/DTPA NP and CSVE/HA/DTPA/Cmab NP. _____	129
Figure 5.7 The XRD spectra of CBT, CSVE, TPGS, HA, CSVE/HA NP, CSVE/HA/DTPA NP and CSVE/HA/DTPA/Cmab NP. _____	130
Figure 5.8 The DSC spectra of CBT, CSVE, TPGS, HA, CSVE/HA NP, CSVE/HA/DTPA NP and CSVE/HA/DTPA/Cmab NP. _____	132

Figure 5.9 The XPS spectra of CSO/HA NP, CSVE/HA NP, CSVE/HA/DTPA NP and CSVE/HA/DTPA/Cmab NP.	132
Figure 5.10 Drug release profile of CSVE/HA/DTPA NP and CSVE/HA/DTPA/Cmab NP in pH 7.4 phosphate buffer saline, pH 5.5 acetate buffer, and pH 5.5 acetate buffer and Glutathione (10 mM).	134
Figure 5.11 Time-dependent change in free thiol concentration in CSVE/HA/DTPA NP suspension after incubation with Acetate buffer (pH 5.5) and GSH	134
Figure 5.12 Effect of the storage of Lyophilized nanoparticles on Hydrodynamic size, PDI, Zeta Potential, and Entrapment Efficiency Data presented as Mean \pm SD (vertical bars); n=6. ns (p-value > 0.05)	138
Figure 5.13 <i>In vitro</i> cell viability of MDA-MB-231 cells after treatment with Cabazitaxel-loaded formulations for 24 h. Data presented as Mean \pm SD (vertical bars); n=6.	139
Figure 5.14 <i>In vitro</i> cell viability of HCT116 cells after treatment with Cabazitaxel-loaded formulations for 24 h. Data presented as Mean \pm SD (vertical bars); n=6.	140
Figure 5.15 <i>In vitro</i> cell viability of T47D cells after treatment with Cabazitaxel-loaded formulations for 24 h (n=6).	141
Figure 5.16 Fluorescence microscopy images of MDA-MB-231 cells after 6 h incubation with the fluorescent CM6-loaded formulations. The blue fluorescence from DAPI channels shows Hoechst 33342 stained nuclei while the third column shows an overlay image of Hoechst and GFP. The fourth column represents an overlay image of phase contrast, GFP, and Hoechst 33342. Each scale bar represents 100 μ m. GFP channel showing higher level of green fluorescence in CM6 loaded CSVE/HA/DTPA/Cmab NP treated cells compared to free CM6 and CM6-loaded CSVE/HA/DTPA NP treated cells due to receptor-mediated cellular uptake of CM6 in the cytoplasm. The CM6-loaded CSVE/HA NP also exhibited superior intracellular localization of CM6 compared to CM6-	

loaded CSO/HA NP which may be attributed to the amphiphilic nature of the CSVE conjugate. The C-mab pretreated cells exhibited reduced uptake of CM6 which may be due to the competitive binding of C-mab to the EGFR. _____ 142

Figure 5.17 Quantitative assessment of intracellular uptake of green fluorescent CM6 in MDA-MB-231 cells treated with free CM6, CSO/HA NP, CSVE/HA NP, CSVE/HA/DTPA NP, CSVE/HA/DTPA/C-mab NP, C-mab pre-treated CSVE/HA/DTPA/C-mab NP at 0.2 $\mu\text{g ml}^{-1}$ concentrations of CM6 for 6 h using flow cytometry. The blue peak shows the highest cellular uptake of CM6 in CM6-loaded CSVE/HA/DTPA/C-mab NP treated cells compared to free CM6, CSO/HA NP, CSVE/HA NP, CSVE/HA/DTPA NP, and CSVE/HA/DTPA/C-mab NP treated cells. _____ 143

Figure 5.18 Assessment of mitochondrial membrane potential by JC-1 dye in control and treated MDA-MB-231 cells after treatment with Cabazitaxel, CSVE/HA/DTPA NP, CSVE/HA/DTPA/C-mab NP, and C-mab pretreated CSVE/HA/DTPA/C-mab NP. The CSVE/HA/DTPA/C-mab NP treated group showed maximum depolarization (green fluorescence of JC-1 monomer) in cells. In contrast, the control group exhibited an accumulation of JC-1 monomers in negatively charged and energized normal mitochondria to spontaneously form J aggregates (Red fluorescence). _____ 144

Figure 5.19 Quantitative detection of mitochondrial membrane potential in MDA-MB-231 after treatment with the formulations through flow cytometry. The upper right and lower right quadrants represent cells with normal mitochondrial membrane potential and depolarized mitochondria respectively. _____ 145

Figure 5.20 Pattern of mitochondrial distribution in MDA-MB-231 cells using Mitotracker™ Red after treatment with Cabazitaxel, CSVE/HA/DTPA NP, CSVE/HA/DTPA/C-mab NP, and C-mab pretreated CSVE/HA/DTPA/C-mab NP. The uniform distribution of mitochondria was seen in control cells represented by the yellow

arrow while aggregated mitochondria were observed in the treatment group represented by the white arrows. The CSVE/HA/DTPA/Cmab treated cells showed the highest mitochondrial aggregation. _____ 147

Figure 5.21 Combined images of Hoechst33342/PI-stained MDA-MB-231 cells after treatment with the formulations. The yellow, white, and red arrows represent early apoptotic, late apoptotic, and necrotic cells. Cells emitting blue fluorescence are Hoechst positive while those with red fluorescence are PI positive. _____ 148

Figure 5.22 Quantitative assessment of apoptosis by AnnexinV/PI dual staining through Flow cytometry in treated MDA-MB-231 cells. AnnexinV/PI dual staining discriminates the percentage of live (lower left quadrant), early apoptotic (lower right quadrant), late apoptotic (upper right quadrant), and necrotic or dead cells (upper left quadrant). ____ 149

Figure 5.23 Concentration of Cabazitaxel in plasma, tumor, liver, lung, spleen and kidney after intravenous administration of Cabazitaxel, CSVE/HA/DTPA NP, and CSVE/HA/DTPA/Cmab NP. Data presented as Mean \pm SD (vertical bars); n=12. ____ 153

Figure 5.24 Body weight and tumor volume of normal SD rats, tumor-bearing SD rats, and formulation treated tumor-bearing SD rats over the 28 days treatment period. Data presented as Mean \pm SD (vertical bars); n=5. _____ 155

Figure 5.25 Images of the tumors harvested from various treatment groups after end of 28-day treatment period. The line marked on the left side of tumor represents a cm-scale. _____ 155

Figure 5.26 Survival rates of tumor-bearing SD rats after treatment with formulations, day 0 represents the day of administration of first dose after the tumor volume reached \sim 500 mm³. _____ 156

Figure 5.27 (A) Histological assessments of tumors isolated from rats after tumor regression study using H&E stain (magnification 4 \times ; scale bar 100 μ m) **(B)** Histological

images of organ tissues after 28 days of treatment regimen. Invasive carcinoma (IC), stromal tissue (ST), proliferated and expanded terminal lobular units (HLU), dilated ducts with inspissated secretions (D), Ductal Carcinoma (DC), Mucin (yellow arrow), Fibroadenoma (F) and breast hyperplasia (H). _____	157
Figure 5.28 Graphical Summary of Objective 2 _____	159
Figure 6.1 Schematic representation of the a) Succinylation of TPGS, b) synthesis of hyaluronic acid–oleylamine conjugate (HA-OA), and c) synthesis of chitosan–oleic acid conjugate (CS-OA). _____	166
Figure 6.2 Schematic representation of the preparation of non-targeted HA-OA/CS-OA based nanoparticles (HA-OA/CS-OA NPT), targeted HA-OA/CS-OA based nanoparticles (HA-OA/CS-OA NPT), free Cabazitaxel drug loaded microneedles (CBT-MN) and targeted HA-OA/CS-OA based nanoparticles loaded microneedles (HA-OA/CS-OA NPT – MN). _____	170
Figure 6.3 ¹ H NMR spectra of Hyaluronic acid, oleylamine (OA), and HA-OA. _____	179
Figure 6.4 ¹ H NMR spectra of Chitosan (CSO), Oleic acid (OA), and CS-OA. _____	180
Figure 6.5 FTIR spectrum of CS, CS-OA, HA, HA-OA, TPGS, and TPGS-COOH _____	181
Figure 6.6 Characterization of HA-OA/CS-OA based hybrid nanoparticles; (A) TEM image of HA-OA/CS-OA NP (B) AFM image of HA-OA/CS-OA NP, (C) TEM image of HA-OA/CS-OA NPT, and (D) AFM image of HA-OA/CS-OA NPT. _____	184
Figure 6.7 (A) FTIR and (B) XRD spectra of CBT, HA-OA/CS-OA NP, HA-OA/CS-OA NPT, and HA-OA/CS-OA NPT MN. _____	185
Figure 6.8 (A) DSC thermogram of CBT, HA-OA/CS-OA NP, HA-OA/CS-OA NPT, and HA-OA/CS-OA NPT-MN. (B) Surface characterization by XPS analysis of HA-OA/CS-OA NP and HA-OA/CS-OA NPT. (C) <i>In vitro</i> drug release study of HA-OA/CS-OA NP and HA-OA/CS-OA NPT at pH 5.8 and pH 7.4. _____	186

Figure 6.9 *In vitro* cytotoxicity of HA-OA/CS-OA NP and HA-OA/CS-OA NPT in MDA-MB 231 breast cancer cell line after 24 hours of treatment. Data presented as Mean 189

Figure 6.10 Fluorescence microscopy images of MDA-MB-231 cells after 6 hours incubation with free C6 and various HA-OA/CS-OA NP, HA-OA/CS-OA NPT, and C-mab-pretreated HA-OA/CS-OA NPT. GFP channel showing a higher level of green fluorescence in HA-OA/CS-OA NP and HA-OA/CS-OA NPT treated cells as compared to free C6. C-mab-pretreated HA-OA/CS-OA NPT treatment showed diminished fluorescence than HA-OA/CS-OA NPT treatment. Images were captured through an inverted fluorescence microscope at 400X magnification and 100 μ m scale bar. 191

Figure 6.11 Combined microscopic images of Hoechst33342 / PI-stained MDA-MB-231 cells after 24 hours of treatment with free CBT, HA-OA/CS-OA NP, HA-OA/CS-OA NPT, and C-mab-pretreated HA-OA/CS-OA NPT. The white, yellow, and red arrows represent early apoptotic, late apoptotic, and necrotic cells. Cells emitting blue fluorescence (DAPI channel) are Hoechst positive while those with red fluorescence (PI channel) are PI positive. 192

Figure 6.12 The impact of free-CBT, HA-OA/CS-OA NP, and HA-OA/CS-OA NPT treatment on the mitochondrial membrane potential of MDA-MB-231 cells was assessed using JC-1 staining after 24 hours of treatment. The increase in green fluorescence emission indicates a decrease in mitochondrial membrane potential upon treatment, with the highest decline seen in HA-OA/CS-OA NPT-treated cells. Red fluorescence indicates normal potential. Cells were examined using an inverted fluorescence microscope at 400X magnification. 194

Figure 6.13 Plot denotes the flow cytometric data of free-CBT, HA-OA/CS-OA NP, and HA-OA/CS-OA NPT treated MDA-MB-231 cells. PI staining was done to determine the percentage of cells in different phases of the cell cycle. HA-OA/CS-OA NPT treated cells

showed a significant ($***p < 0.001$) increase in cell population in the G2-M phase in comparison to the control. A significant difference between various treatment groups was also observed. Free-CBT and HA-OA/CS-OA NP ($***p < 0.001$), free-CBT and HA-OA/CS-OA NPT ($***p < 0.001$), and HA-OA/CS-OA NP and HA-OA/CS-OA NPT ($**p < 0.01$) was observed. _____ 195

Figure 6.14 Photograph and Scanning Electron Microscopy (SEM) images of HA-OA/CS-OA NPT MN _____ 196

Figure 6.15 Microscopic images of HA-OA/CS-OA NPT MN after exposure to PBS pH 7.4 and dissolution of microneedles in PBS pH 7.4 (calculated in terms of percentage therapeutic payload release w.r.t. time). _____ 197

Figure 6.16 Images of parafilm layers after insertion of HA-OA/CS-OA NPT MN. The histogram represents the percentage of holes created in each layer of parafilm by microneedles after manual insertion _____ 199

Figure 6.17 (A) Microscopic image of rat skin after HA-OA/CS-OA NPT MN insertion. **(B)** Graph representing ex vivo drug permeation across rat skin determined using a Franz diffusion cell. HA-OA/CS-OA NPT-MN showed significant improvement in drug permeation in comparison to CBT-MN and HA-OA/CS-OA NPT loaded PVA/HA blend ($****p \text{ value} < 0.001$) **(C)** Representation of percentage drug retention in skin after 48 hours of drug permeation study. _____ 200

Figure 6.18 (A) Tumor regression analysis in Tumor-bearing female SD rats; Tumor volume of control, CBT (i.v.), CBT-MN, and HA-OA/CS-OA NPT-MN treated groups during a 14-day treatment period. **(B)** Image of tumors collected from treatment groups after 14 days of treatment. _____ 203

Figure 6.19 (A) Body weight of healthy female SD rats and tumor-bearing female SD rats receiving CBT (i.v.), CBT-MN, and HA-OA/CS-OA NPT-MN treatment for a 14-day

treatment regimen. **(B)** The Kaplan-Meier survival probability plot (120 days) of Healthy and tumor-bearing female SD rats treated with CBT (i.v.), CBT-MN, and HA-OA/CS-OA NPT-MN treated groups. _____ 203

Figure 6.20 Histological images of H&E stained healthy/tumor tissues before and after 14-day treatment with CBT (i.v.), CBT-MN and HA-OA/CS-OA NPT-MN. _____ 205

Figure 6.21 Graphical Abstract of Objective 3 _____ 206

List of Tables

Table 2.1 Biopolymer for tumor microenvironment responsiveness for site-specificity	21
Table 2.2 Targeted nanomedicine responsive to the tumor microenvironment and their drug release mechanisms	39
Table 4.1 Composition of CS-HA-NP and CS-HA-Cmab-NP nanoparticles	59
Table 4.2 Interpretation of ¹ H NMR Spectra of TPGS and TPGS-COOH	69
Table 4.3 Interpretation of ¹³ C NMR Spectra of TPGS and TPGS-COOH	71
Table 4.4 Interpretation of the mass (TOF) spectra of TPGS and TPGS-COOH	78
Table 4.5 Characterization of CS-HA-NP and CS-HA-Cmab-NP nanoparticles	81
Table 4.6 XPS surface atomic percentage of N1s, O1s, C1s, S2p, and P2p in CS-HA-NP and CS-HA-Cmab-NP	85
Table 4.7 Correlation coefficients of Cabazitaxel release profile from CS-HA-NP and CS-HA-Cmab-NP at various pH in various fitted release kinetic models	87
Table 4.8 Pharmacokinetic parameters of Neat CBT, CS-HA-NP, and CS-HA-Cmab-NP after I.V. administration (6.5 mg/kg IV, n = 12) in female Sprague Dawley rats.	96
Table 5.1 Composition, particle size, polydispersity index (PDI), zeta potential, and entrapment efficiency of various formulations.	127
Table 5.2 R-square values for mathematical models to determine the goodness of fit.	137
Table 5.3 Pharmacokinetic parameters of various formulations determined from plasma concentration vs time plot	151
Table 6.1 Composition and properties of various HA-OA/CS-OA NPs prepared during optimization	168
Table 6.2 Composition of the various formulations used to prepare MNs	169
Table 6.3 Particle size, PDI, zeta potential, EE, and DL of prepared nanoparticles.	183
Table 6.4 Fitted release kinetic model for in-vitro drug release of nanoparticles.	188

LIST OF ABBREVIATIONS

- EPR** : Enhanced permeation and retention effect
- i.v.** : Intravenous
- VES** : Vitamin-E succinate
- CSO** : Chitosan oligosaccharide
- CS** : Chitosan
- HA** : Hyaluronic acid
- NaTPP**: Sodium tripolyphosphate
- EDAC / EDC** : 1-Ethyl-3-(3-Dimethylaminopropyl)carbodiimide Hydrochloride
- NHS** : N-hydroxysuccinimide
- Sulfo-NHS**: N-hydroxysulfosuccinimide
- DTPA** : 3,3'-dithiodipropionic acid
- CBT** : Cabazitaxel
- PDI** : Polydispersity Index
- DLS** : Dynamic Light Scattering
- FTIR** : Fourier Transform Infrared Spectroscopy
- SEM** : Scanning Electron Microscope
- SPM** : Scanning Probe Microscope
- AFM** : Atomic Force Microscope
- HR-TEM**: High-Resolution Transmission Electron Microscope
- XRD** : Powder X-ray diffraction
- DSC** : Differential Scanning Calorimetry
- XPS** : X-ray Photoelectron Spectroscopy
- TPGS** : Tocopherol polyethylene glycol succinate
- PBS** : Phosphate Buffer Saline

FBS : Fetal Bovine Serum

MTT : (3-(4, 5-dimethylthiazolyl-2)-2, 5-diphenyltetrazolium bromide)

DCFDA: 2'-7'- dichlorodihydrofluorescein diacetate

JC-1 : 5,5',6,6'-tetrachloro-1,1',3,3'-tetraethylbenzimidazolylcarbocyanine iodide

PI : Propidium Iodide

DAPI : 4',6-diamidino-2-phenylindole

DMBA: 7,12-Dimethylbenz[a]anthracene

H&E : Hematoxylin and eosin staining

AUC : Area Under Curve

MRT : Mean Residence Time

GSH : Glutathione

ROS : Reactive Oxygen Species

IC₅₀ : Half maximal inhibitory concentration

C6 : Coumarin-6

Cmab : Cetuximab

Preface

Cancer remains one of the leading causes of mortality worldwide, posing significant challenges to healthcare systems and researchers alike. Despite numerous advancements in cancer therapy, the effective delivery of therapeutic molecules to cancer cells remains a significant hurdle. Traditional chemotherapeutics often suffer from poor aqueous solubility and limited availability at the intended region. Recognizing these challenges, researchers are delving into developing tumor microenvironment (TME)--responsive nanomedicine as a promising strategy for breast cancer therapy. This approach leverages the unique characteristics of the TME, such as lower pH, reactive oxygen species (ROS), redox imbalance, hypoxia, and enzymatic activity, to achieve targeted and controlled drug release, thereby enhancing treatment efficacy while minimizing systemic toxicity.

Chapter 1 provides an introduction to the biopolymer-based therapeutic approaches for targeted delivery of chemotherapeutics in breast cancer.

Chapter 2 comprehensively discusses various strategies employed in recent years to develop targeted therapeutic carriers that selectively deliver the drugs to cancerous cells.

Chapter 3 outlines the objectives and plan of work.

Chapter 4 focuses on preparing and characterizing HA-stabilized chitosan (CS) nanoparticles using the ionic gelation method. These nanoparticles were designed to entrap cabazitaxel (CBT), a potent chemotherapeutic agent, and were functionalized with Cetuximab (Cmab) to target epidermal growth factor receptors (EGFR) overexpressed on cancer cells. The nanoparticles were evaluated for various physicochemical characteristics, followed by *in vitro* and *in vivo* evaluation. *In vitro* studies demonstrated enhanced cytotoxicity, cellular uptake, and cellular responses, including mitochondrial depolarization and nuclear condensation, due to receptor-mediated endocytosis. The nanoparticles also showed improved pharmacokinetic performance and *in vivo* anti-tumor

efficacy, with minimal organ toxicity, highlighting their potential as effective drug carriers for targeted cancer therapy.

Chapter 5 covers the synthesis of chitosan oligosaccharide and vitamin E succinate conjugate, its evaluation, and its application in the development of a novel GSH-responsive Cetuximab-anchored chitosan/vitamin-E succinate conjugate-based hybrid nanoparticle. The chapter subsequently covers the characterization and evaluation of these spherical, sub-200 nm, cationic, and redox-responsive nanoparticles. *In vitro* evaluations showed significantly higher cytotoxicity against MDA-MB-231 cells, enhanced cellular uptake, and reduced mitochondrial membrane potential compared to free CBT. The *in vivo* pharmacokinetic studies indicated better performance of the nanoparticles, with improved half-life, area under the curve (AUC), and mean residence time (MRT). Further, the chapter discussed the tumor regression, survival, and histological data confirming these nanoparticles' efficacy and safety, demonstrating their potential as a targeted anticancer drug delivery platform.

Chapter 6 delves into the fabrication of targeted nanoparticles-loaded microneedles for localized drug delivery of cabazitaxel in DMBA-induced tumor-bearing SD rats. The article focuses on developing chitosan and hyaluronic acid-based amphiphilic conjugates with similar hydrophobic fragments. The fabrication of deformable HA-OA/CS-OA-based nanoparticles and loading of these particles in PVA/HA-based dissolving microneedles, followed by its *in vitro* and *in vivo* evaluation, forms the basic premise of this chapter.

Chapter 7 outlines the summary, conclusions, shortfalls, and future perspectives of all the objectives undertaken.

Chapter 8 lists all the references utilized to conduct this research.

Appendices provide a list of key publications from the work done during the doctoral research, and the first page of the publications from the work discussed in the thesis has been included.